ELSEVIER

Computers and Geotechnics 23 (1998) 131–164

COMPUTERS AND GEOTECHNICS

Consequences of the t_{ij}-concept and a new modeling approach

E.Q. Chowdhury [a,*], T. Nakai [b]

[a] *Department of Civil Engineering, Nagoya Institute of Technology, Gokiso-cho, Showa-ku, Nagoya 466, Japan*

[b] *Department of Systems Management and Engineering, Nagoya Institute of Technology, Gokiso-cho, Showa-ku, Nagoya 466, Japan*

Received 5 January 1998; received in revised form 23 April 1998; accepted 25 April 1998

Abstract

The strength and the dilatancy of soils are largely influenced by the choice of the stress and strain increment variables. Cam-clay like models that use extended Mises strength criterion cannot consider the effect of intermediate principal stress properly and give unrealistic strength under generalized three-dimensional stresses except triaxial compression condition. Nakai and Mihara proposed a modified stress tensor (t_{ij}) based on the Spatially Mobilized Plane (SMP) concept that uses Matsuoka–Nakai strength criterion to consider the influence of intermediate principal stress on the strength and the dilatancy of soils. Matsuoka–Nakai strength criterion is a convex surface on the π-plane in the ordinary stress space and satisfies Mohr–Coulomb criterion under axisymmetric conditions (triaxial compression and extension). Using the t_{ij}-concept, isotropic and kinematic hardening clay and sand models have been proposed and experimentally verified. Recent investigations have revealed inconsistency of the t_{ij}-concept with the critical state concept used in the original and modified Cam-clay models. In this paper the inconsistency of the t_{ij}-concept with the critical state concept is pointed out first, then a modeling approach has been introduced, which virtually can adopt any strength criterion in a consistent way to incorporate the critical state concept. It is shown that the proposed stress and strain increment quantities are properly work conjugate. A compact stress–dilatancy relation is also introduced using the proposed stress and strain increment quantities, which gives a continuous and smooth plastic potential and has control over the stiffness of the model predictions.

* Corresponding author. Fax: 81 52 735 5485; e-mail: eqc@tuti1.ace.nitech.ac.jp

0266-352X/99/$—see front matter
PII: S0266-352X(98)00017-2

1. Introduction

Numerous constitutive models for soils have been proposed to simulate various aspects of soil behavior but many of them use extended Mises type failure criteria as in Eq. (1) like the Cam clay [1,2]. Throughout this paper 'Cam-clay models' refers to the models proposed by Roscoe et al. (1963) and Roscoe and Burland (1968).

$$\eta = q/p = \text{constant}, \tag{1}$$

where p and q are the effective mean and the deviator stresses given by the following two equations.

$$p = \sigma_{ij}\delta_{ij}/3, \tag{2}$$

$$q = \sqrt{3/2(\sigma_{ij} - p\delta_{ij})(\sigma_{ij} - p\delta_{ij})}. \tag{3}$$

It is to be noted that all stresses mentioned in this paper are effective stresses.

The experimental evidence shows that the strength of soil under triaxial extension and true triaxial conditions are much less than those predicted by the extended Mises criterion. Lade–Duncan [3] and Matsuoka–Nakai [4] proposed the failure criteria as in Eqs. (4) and (5) respectively to predict the strength of soils under three-dimensional stress conditions.

$$J_1^3/J_3 = \text{constant}, \tag{4}$$

$$X_f = \sqrt{J_1J_2/(9J_3) - 1} = \text{constant} \quad \text{or} \quad J_1J_2/J_3 = \text{constant}, \tag{5}$$

where X_f is the stress ratio at failure according to the Spatially Modified Plane (SMP) concept [Eqs. (7)–(9)]. In the above equations J_1, J_2 and J_3 are the first, second and the third invariants of effective stresses. Various strength criteria are plotted on the deviator plane in Fig. 1. The axes I, II and III indicate the principle directions. It can be seen from this figure that Matsuoka–Nakai strength surface circumscribes the Mohr–Coulomb pyramid and gives the same angle of internal friction at triaxial compression and extension. While, Lade–Duncan criterion gives higher strength under triaxial extension than compression ($\phi'_{\text{fext}} > \phi'_{\text{fcomp}}$), but much below than that predicted by the extended Mises criterion.

The Matsuoka–Nakai failure criterion [Eq. (5)] has been evolved from the SMP concept [4]. The direction cosines of the normal to the SMP are given by Eq. (6).

$$a_i = \sqrt{J_3/(J_2\sigma_i)}. \tag{6}$$

The normal (σ_{SMP}) and the shear (τ_{SMP}) stresses on the SMP can be obtained as in Eqs. (7) and (8) respectively and the stress ratio (X) is given by Eq. (9).

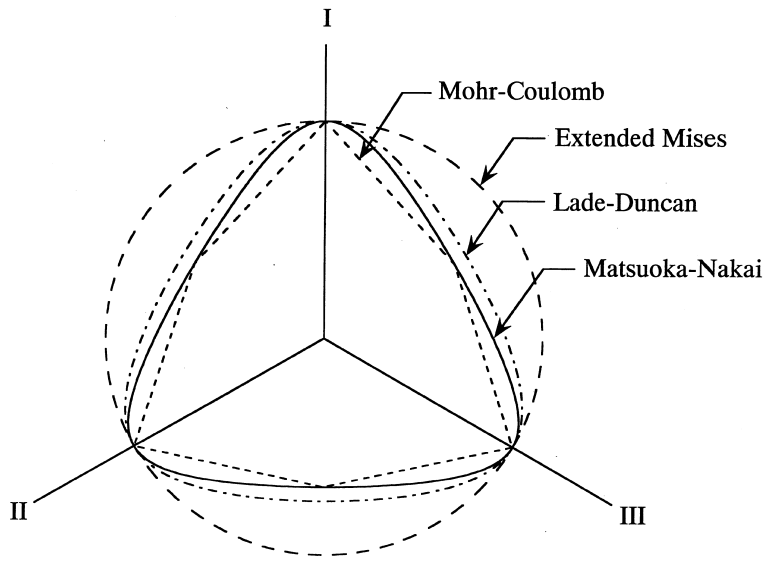

Fig. 1. π-plane sections of various failure surfaces in the ordinary stress space.

$$\sigma_{\mathrm{SMP}} = \sigma_1 a_1^2 + \sigma_2 a_2^2 + \sigma_3 a_3^3 = 3J_3/J_2, \tag{7}$$

$$\tau_{\mathrm{SMP}} = \sqrt{\sigma_1^2 a_1^2 + \sigma_2^2 a_2^2 + \sigma_3^3 a_3^3 - \sigma_{\mathrm{SMP}}^2} = \left(\sqrt{J_1 J_2 J_3 - 9J_3^2}\right)_2, \tag{8}$$

$$X = \tau_{\mathrm{SMP}}/\sigma_{\mathrm{SMP}} = \sqrt{J_1 J_2/(9J_3) - 1}. \tag{9}$$

Using the extended SMP concept [5], the ordinary strain increment vector (**d**) can be resolved as the strain increment components normal ($\mathrm{d}_{\mathrm{SMP}}{}^*$) and parallel ($\mathrm{d}\gamma_{\mathrm{SMP}}{}^*$) to the SMP as in Eqs. (10) and (11) respectively.

$$\mathrm{d}\varepsilon^*_{\mathrm{SMP}} = \mathrm{d}\varepsilon_1 a_1 + \mathrm{d}\varepsilon_2 a_2 + \mathrm{d}\varepsilon_3 a_3, \tag{10}$$

$$\mathrm{d}\gamma^*_{\mathrm{SMP}} = \sqrt{\mathrm{d}\varepsilon_1^2 + \mathrm{d}\varepsilon_2^2 + \mathrm{d}\varepsilon_3^3 - \left(\mathrm{d}\varepsilon^*_{\mathrm{SMP}}\right)^2}. \tag{11}$$

The above interpretation was given in the principal stress space. Later, Nakai–Mihara [6] have given a more generalized interpretation for the three-dimensional stress conditions. They defined a tensor called modified stress tensor (t_{ij}) that is given by Eq. (12).

$$t_{ij} = a_{ik}\sigma_{kj}, \tag{12}$$

where a_{ij} is a dimensionless symmetric tensor whose principal values ($\hat{a}_{ij}$) are the direction cosines of the SMP and are given by Eq. (6). The generalized tensor a_{ij} can be calculated by reverse tensor transformation [7] as follows:

$$a_{ij} = Q_{im}Q_{jn}\hat{a}_{mn}, \tag{13}$$

where Q_{ij} is an orthogonal tensor which transforms ordinary stress tensor (σ_{ij}) to its Eigen values ($\hat{\sigma}_{ij}$).

$$\hat{\sigma}_{ij} = Q_{mi}Q_{nj}\sigma_{mn}. \tag{14}$$

The normal (t_N) and the parallel (t_S) components of the modified stresses (t_{ij}) to the SMP and the stress ratio (X) are given by Eqs. (15)–(17) respectively [8].

$$t_N = t_{ij}a_{ij} = 3J_3/J_2 \equiv \sigma_{SMP}, \tag{15}$$

$$t_S = \sqrt{(t_{ij} - t_N a_{ij})(t_{ij} - t_N a_{ij})} = \left(\sqrt{J_1J_2J_3 - 9J_3^2}\right)J_2 \equiv \tau_{SMP}, \tag{16}$$

$$X = t_S/t_N = \sqrt{J_1J_2/(9J_3) - 1} \equiv \tau_{SMP}/\sigma_{SMP}. \tag{17}$$

Strain increments are given in a generalized way by the following equations, which are equivalent to Eqs. (10) and (11) respectively.

$$d\varepsilon^*_{SMP} = d\varepsilon_{ij}a_{ij}, \tag{18}$$

$$d\gamma^*_{SMP} = \sqrt{(d\varepsilon_{ij} - d\varepsilon^*_{SMP}a_{ij})(d\varepsilon_{ij} - d\varepsilon^*_{SMP}a_{ij}}. \tag{19}$$

Using the above stress and strain rate variables isotropic and kinematic hardening clay and sand models have been proposed by Nakai et al. [8,9,10,11] and verified by various tests on clay and sand. These models could successfully predict various aspects of soil behavior.

But the models using t_{ij}-concept are inconsistent with the critical state concept that is used in the original and the modified Cam-clay models due to the different shapes of the yield and the critical state surfaces. In the t_{ij}-clay model, the dilatancy Y is defined as

$$Y = d\varepsilon^{*p}_{SMP}d\gamma^{*p}_{SMP}, \tag{20}$$

where superscript p in the strain increment quantities stands for plastic strains. Since, the strain increment quantities $d\varepsilon^{*p}_{SMP}$ and $d\gamma^{*p}_{SMP}$ are not only the functions of ordinary plastic strain increments but also depend on the relative magnitude of intermediate principal stress [see Eqs. (10), (11), (18) and (19)], the dilatancy is dependent on the stress condition in general. Eq. (21) is the linear stress–dilatancy relation proposed in the original t_{ij}-clay model [8].

$$Y = d\varepsilon^{*p}_{SMP}d\gamma^{*p}_{SMP} = (M^* - X)/\alpha \tag{21}$$

Soil parameter α indicates the slope of stress–dilatancy curve and M^* is the stress ratio (X) at zero dilatancy ($Y = 0$) and can be evaluated from Eq. (22) by substituting the critical values of stress ratio ($X = X_f$) and dilatancy ($Y = Y_f$) in Eq. (21).

$$M^* = X_f + \alpha Y_f. \tag{22}$$

Values of X_f and Y_f are calculated considering triaxial compression condition and using Eqs. (6), (9), (10) and (11). Finally they take the forms as in Eqs. (23) and (24) respectively. Where R is the major–minor principal stress ratio ($R = \sigma_1/\sigma_3$) and the subscript f_{comp} denotes the critical state under triaxial compression.

$$X_f = \frac{\sqrt{2}}{3}\left(\sqrt{R_{fcomp}} - \frac{1}{\sqrt{R_{fcomp}}}\right) \tag{23}$$

$$Y_f = \frac{1}{\sqrt{2}}\frac{\left(1 - \sqrt{R_{fcomp}}\right)}{\left(\sqrt{R_{fcomp}} + 0.5\right)} \tag{24}$$

If the triaxial extension condition is considered, above equations become

$$X_f = \frac{\sqrt{2}}{3}\left(\sqrt{R_{fext}} - \frac{1}{\sqrt{R_{fext}}}\right) \tag{25}$$

$$Y_f = \sqrt{2}\frac{\left(1 - \sqrt{R_{fext}}\right)}{\left(\sqrt{R_{fext}} + 2\right)} \tag{26}$$

where R_{fext} is the major–minor principal stress ratio at the critical state under triaxial extension condition. The t_{ij}-concept assumes Matsuoka–Nakai strength criterion, which gives same angles of internal friction under triaxial compression and extension $\left(\phi'_{fcomp} = \phi'_{fext} \text{ or } R_{fcomp} = R_{fext}\right)$. Eqs. (23) and (25) give the same value of X_f under triaxial compression and extension conditions if $R_{fcomp} = R_{fext}$, but the magnitudes of dilatancy at critical states [Eqs. (24) and (26)] are different. Thus, to satisfy the stress–dilatancy relation given by Eq. (21), stress ratio X should take different values at the critical state depending on the relative magnitude of intermediate principal stress.

The critical state is defined in the critical state soil mechanics [12] as a state where very large shear strain is produced without further change in the plastic volumetric strain and without the change of effective stresses. Eq. (27) or (28) can express the Cam-clay critical state conditions.

$$D = \frac{d\varepsilon_v^p}{d\varepsilon_d^p} = 0, \tag{27}$$

$$\frac{\partial g}{\partial \sigma_{kk}} = 0. \tag{28}$$

For the Cam-clay model, at critical state, stress ratio reaches a constant value ($\eta = M$) independent of the stress condition. Equivalent critical state expressions for the t_{ij}-clay model are as follows

$$Y = \frac{\mathrm{d}\varepsilon^{\mathrm{p}}_{\mathrm{SMP}^*}}{\mathrm{d}\gamma^{\mathrm{p}}_{\mathrm{SMP}^*}} = Y_{\mathrm{f}}, \tag{29}$$

$$\frac{\partial g}{\partial t_{kk}} = 0. \tag{30}$$

Since, the value of $Y_{\mathrm{f}}(Y_{\mathrm{f}} \neq 0)$ is dependent on the stress condition, Eq. (29) cannot express the critical state condition uniquely for the t_{ij}-clay model but Eq. (30) still holds. As mentioned above, stress ratio X should take different values to satisfy Eq. (30). In brief, unlike the Cam-clay model ($q/p = \eta = \text{const.}$), the critical state surface of the t_{ij}-clay model is not a constant stress ratio ($t_{\mathrm{S}}/t_{\mathrm{N}} = X \neq \text{const.}$) surface though it gives strengths of normally consolidated clay close to the observed ones under three-dimensional stress conditions. So, the t_{ij}-concept implicitly violates the Matsuoka–Nakai failure criterion, which is a constant stress ratio ($X = \text{const.}$) surface if the critical state concept is incorporated in the t_{ij}-clay model.

The critical state surface [using Eq. (30)] of the t_{ij}-clay model is shown in Fig. 2 along with other failure criteria on the deviator plane. It can be seen from this figure

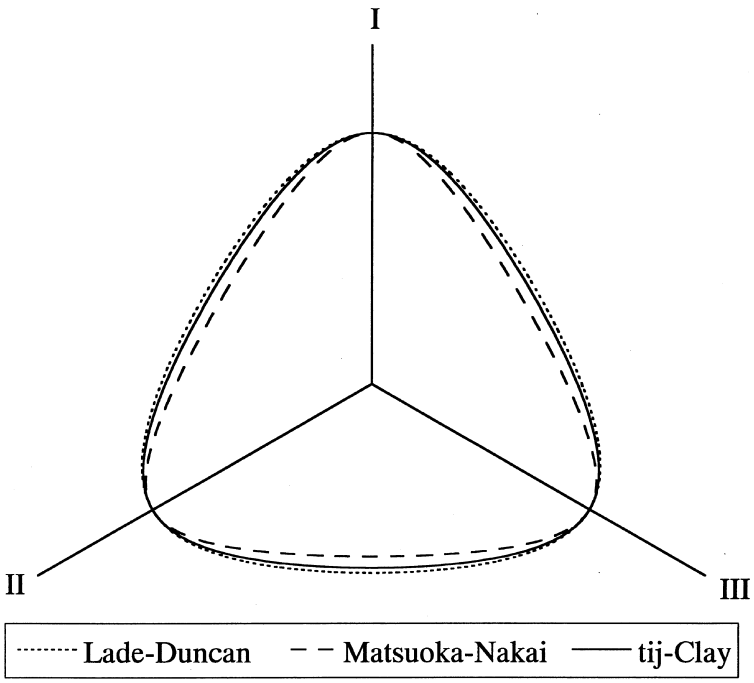

Fig. 2. Lade–Duncan and Matsuoka–Nakai strength surfaces and the critical state surface predicted by the t_{ij}-clay model.

that the critical state surface predicted by the t_{ij}-clay and the Matsuoka–Nakai strength surface are different. Throughout this paper we will restrict our discussion to the normally consolidated clay. According to the critical state concept, critical state surface will coincide with the strength surface for normally consolidated clay. Fig. 3 shows that at the critical state under triaxial compression condition, yield surface ($X=$const.) of the t_{ij}-clay model touches the critical state surface ($\partial g/\partial t_{kk}=0$) at $b=(\sigma_2-\sigma_3)/(\sigma_1-\sigma_3)=0$ but the remaining part of the yield surface lies inside the critical state surface. In case of the triaxial extension, yield surface touches the critical state surface at $b=1$ but the remaining part of the yield surface lies outside the critical state surface. Thus, it is possible to get higher strengths than those that can be obtained by monotonic loading for normally consolidated clay under triaxial compression and true triaxial conditions if stress condition move along the yield surface from triaxial extension towards compression condition by neutral loading (Fig. 3). To avoid such situation, it is required that the shapes of the yield and critical state surfaces should be the same so that the yield and critical state surfaces coincide at the critical state independent of the stress condition.

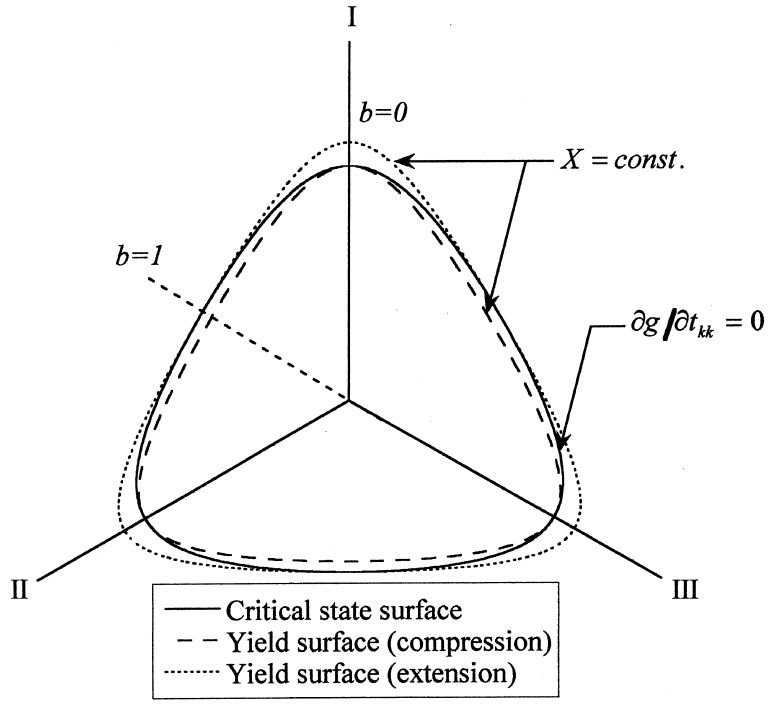

Fig. 3. π-plane sections of the yield surfaces of the t_{ij}-clay model at critical states under triaxial compression and extension and the predicted critical state surface.

Other interpretations of the non-unique yield and critical state surfaces are shown in Fig. 4Fig. 5. The exaggerated critical states predicted by the t_{ij}-clay model are shown on the stress–dilatancy curve under triaxial compression and extension conditions (Fig. 4). Under true triaxial conditions, critical states lie in-between. If a non-linear stress–dilatancy is assumed, then the critical states are different from those shown in Fig. 4. Thus, the critical state surface of the t_{ij}-clay model is also dependent on the shape of the stress–dilatancy curve, which is also a departure from the conventional models like Cam clay. Fig. 5 shows the normal consolidation line (NCL) and the critical state lines (CSL) on the e vs. $\ln(t_N)$ plane, which are usually assumed to be parallel. For the t_{ij}-clay model, two critical state lines (for compression and extension) define the zone of critical states where the critical state lines of the true triaxial conditions lie. While in the Cam-clay models the critical state line is a single line independent of the stress conditions on the e vs. $\ln p$ plane.

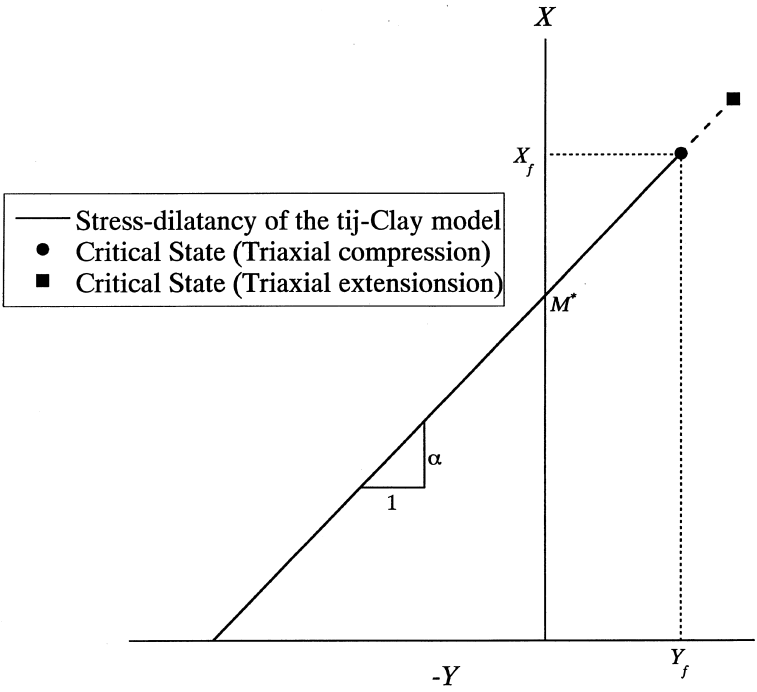

Fig. 4. Predicted critical states under triaxial compression and extension on the stress-dilatancy curve of the t_{ij}-clay model.

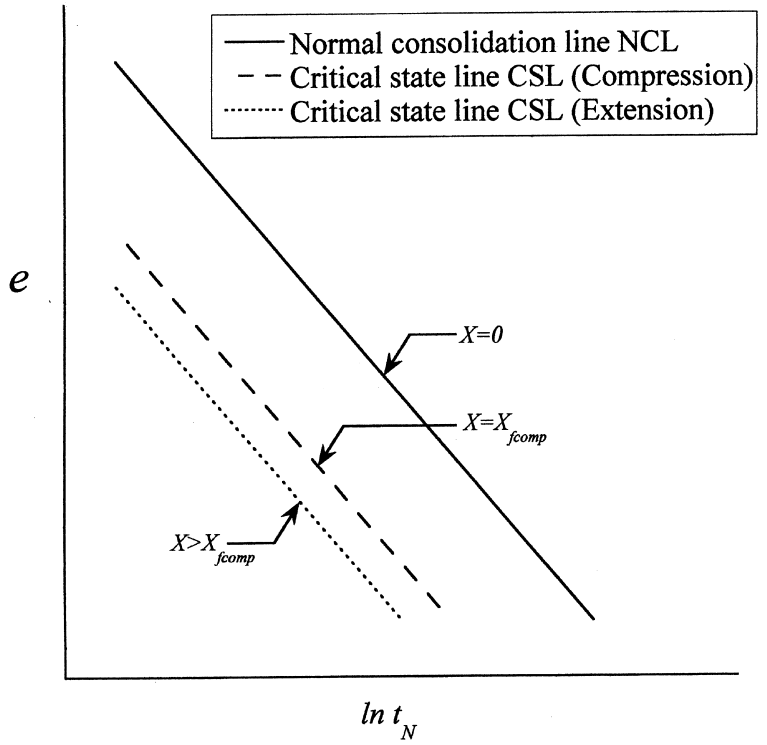

Fig. 5. Qualitative normal consolidation line and the critical state lines of the t_{ij}-clay model on the compression plane.

2. A new modeling approach

2.1. Stress and strain increment quantities

In this section we will introduce new stress quantities, which can consider the influence of intermediate principal stress to any degree, on the strength and the dilatancy of soils. In other words, new stress quantities can incorporate any strength criterion (extended Mises to Mohr–Coulomb) in the elastoplastic modeling of soil behavior in a consistent way while, retaining all elements of the critical state concept. We will also show that the new stress and strain increment quantities are properly work conjugate.

Let, the new stress quantities be called modified stress (τ_{ij}), which is a symmetric tensor and whose principal directions are coaxial with the principal directions of the ordinary stress and can be obtained from the ordinary stress (σ_{ij}) in a similar way as the t_{ij} [6] as follows:

$$\tau_{ij} = b_{ik}\sigma_{kj}, \tag{31}$$

where the tensor b_{ij} is a dimensionless symmetric tensor and function of the ordinary stress σ_{ij} and its invariants, which plays the main role in this new approach. Explicit expressions for b_{ij} will be shown later. Let, the mean (τ_m) and the deviator (τ_s) components of the modified stress are the measures of normal and shearing stresses, which are given by the following two equations. The stress ratio (χ) is given by Eq. (34).

$$\tau_m = \tau_{ij}\delta_{ij}/3 \tag{32}$$

$$\tau_s = \sqrt{(\tau_{ij} - \tau_m\delta_{ij})(\tau_{ij} - \tau_m\delta_{ij})} \tag{33}$$

$$\chi = \tau_s/\tau_m \tag{34}$$

The generalized strength criterion can then be given by Eq. (35), which forms a circle on the deviator plane in the modified stress space τ_{ij} for the feasible expressions of b_{ij} and forms circular or the shapes like Matsuoka–Nakai or Lade–Duncan surfaces on the deviator plane in the ordinary stress space.

$$\chi = \tau_s/\tau_m = \text{const.} \tag{35}$$

Since, the principal directions of the modified stress (τ_{ij}) and the principal directions of the plastic strain increments are coaxial with the principal directions of the ordinary stress (σ_{ij}), strain increment quantities conjugate to the stress quantities τ_m and τ_s can be given by the ordinary volumetric (d_v) and the deviator (d_s) strain increments [Eqs. (36) and (37)] respectively. These strain increment quantities are free from stress ratio terms; hence, the dilatancy at the critical state will be unique. Thus, the π-plane sections of the yield, plastic potential and the critical state surfaces will coincide at the critical state independent of the stress conditions.

$$d\varepsilon_v = d\varepsilon_{ij}\delta_{ij}/3, \tag{36}$$

$$d\varepsilon_s = \sqrt{(d\varepsilon_{ij} - d\varepsilon_v\delta_{ij}/3)(d\varepsilon_{ij} - d\varepsilon_v\delta_{ij}/3)}. \tag{37}$$

The above equations are summarized and compared with those of the Cam clay and the t_{ij}-clay models in Table 1. We will formulate a simple elastoplastic model using these stress and strain increment quantities in a later section.

2.2. *Determination of* b_{ij}

There are debates over what should be the failure surface for soils. But one thing is well established that the strengths of soils under triaxial extension and true triaxial conditions should be much below than those predicted by the extended Mises criterion. Without any further controversy we will show that any failure surface can be incorporated in the modeling by using the proposed concept.

Table 1
Comparison between various stress and strain increment variables

Cam Clay	t_{ij}-Clay	Proposed
σ_{ij}	$t_{ij} = a_{ik}\sigma_{kj}$	$\tau_{ij} = b_{ik}\sigma_{kj}$
δ_{ij} (identity tensor)	a_{ij}	b_{ij}
$p = \sigma_{ij}\delta_{ij}/3$	$t_N = t_{ij}a_{ij}$	$\tau_m = \tau_{ij}\delta_{ij}/3$
$S_{ij} = \sigma_{ij} - p\delta_{ij}$	$t'_{ij} = t_{ij} - t_N a_{ij}$	$\tau'_{ij} = \tau_{ij} - \tau_m\delta_{ij}$
$q = \sqrt{(3/2)s_{ij}s_{ij}}$	$t_S = \sqrt{t'_{ij}t'_{ij}}$	$\tau_s = \sqrt{\tau'_{ij}\tau'_{ij}}$
$\eta_{ij} = s_{ij}/p$	$x_{ij} = t_{ij}/t_N$	$\chi_{ij} = \tau_{ij}/\tau_m$
$\eta = q/p = \sqrt{(3/2)\eta_{ij}\eta_{ij}}$	$X = t_S/t_N = \sqrt{x_{ij}x_{ij}}$	$\chi = \tau_s/\tau_m = \sqrt{\chi_{ij}\chi_{ij}}$
$d\varepsilon_v = d\varepsilon_{ij}\delta_{ij}$	$d\varepsilon^*_{SMP} = d\varepsilon_{ij}a_{ij}$	$d\varepsilon_v = d\varepsilon_{ij}\delta_{ij}$
$d\varepsilon'_{ij} = d\varepsilon_{ij} - \delta_{ij}d\varepsilon_v/3$	$de_{if} = d\varepsilon_{ij} - d\varepsilon^*_{SMP}a_{ij}$	$d\varepsilon'_{ij} = d\varepsilon_{ij} - \delta_{ij}\,d\varepsilon_v/3$
$d\varepsilon_d = \sqrt{2/3\ d\varepsilon'_{ij}\ d\varepsilon'_{ij}}$	$d\gamma^*_{SMP} = \sqrt{de_{ij}\ de_{ij}}$	$d\varepsilon_s = \sqrt{d\varepsilon'_{ij}\ d\varepsilon'_{ij}}$
$d\varepsilon^p_{ij} = \Lambda\ (\partial g/\partial\sigma_{ij})$	$d\varepsilon^p_{ij} = \Lambda\ (\partial g/\partial t_{ij})$	$d\varepsilon^p_{ij} = \Lambda\ (\partial g/\partial t_{ij})$

The tensor b_{ij} plays the most vital role in the proposed concept because it controls not only the shape of the failure surface but also the yield and the plastic potential surfaces. If the principal values of the tensor b_{ij} are denoted by $\hat{b}_{ij}$, then b_{ij} can be obtained by the reverse transformation as follows:

$$b_{ij} = Q_{im}Q_{jn}b_{mn}. \tag{38}$$

To define the principal values of b_{ij} following guidelines must be considered.

(a) (a) If the principal effective stresses are such that $\hat{\sigma}_{11} \geqslant \hat{\sigma}_{22} \geqslant \hat{\sigma}_{33}$ then the principal values of b_{ij} should satisfy $\hat{b}_{11} \leqslant \hat{b}_{22} \leqslant \hat{b}_{33}$.
(b) (b) Failure surface should be smooth, convex and the π-plane sections in the ordinary stress space should coincide or lie in between extended Mises and a surface circumscribing Mohr–Coulomb surface (Matsuoka–Nakai criterion for example).
(c) (c) The stress–dilatancy relation or the stress–strain curve should match the observed response.

There may be many functions that can be assumed for the principal values of b_{ij} satisfying the first condition. For example

$$\hat{b}_{ij} = \begin{cases} K\left(J_1/\hat{\sigma}_{ij}\right)^m & (\text{if } i = j), \\ 0 & (\text{if } i \neq j), \end{cases} \tag{39}$$

$$\hat{b}_{ij} = \begin{cases} K\left(1 - \hat{\sigma}_{ij}/J_1\right)^m & (\textit{if } i = j), \\ 0 & (\textit{if } i \neq 0). \end{cases} \tag{40}$$

In the above equations J_1 is the first invariant of effective stresses (σ_{ij}), $\hat{\sigma}_{ij}$ are the principal values of the ordinary stress and K is a proportionality constant that can be evaluated from Eq. (41). That is, we are restricting the magnitude of b_{ij} to one, which is not a necessity.

$$|b| = \sqrt{b_{ij}b_{ij}} = 1. \tag{41}$$

Changing the value of the exponent m of the above two equations and using Eq. (35), a wide variety of failure surfaces can be generated. Fig. 6(a) and (b) show the failure surfaces on the deviator plane of the ordinary stress space generated by Eq. (35) and using Eqs. (39) and (40) respectively. For both Eqs. (39) and (40), failure surfaces coincide with the extended Mises criterion for $m=0$ and approache to circumscribe the Mohr–Coulomb pyramid as m increases. The strength surface using Eq. (39) approaches to circumscribe Mohr–Coulomb surface for m value close to one. If m becomes exactly equal to one, strength surface becomes a point, which is meaningless. Also, it is numerically verified using Eq. (39) that the stress-strain curves are too flexible, which do not resemble the experimental observations. So, from now on, we shall consider Eq. (40) as one of the appropriate expressions for the principal values of b_{ij}, which can also be written as follows:

$$\hat{b}_{ij} = \begin{cases} \dfrac{(1-\hat{\sigma}_{ij}/J_1)^m}{\sqrt{(1-\hat{\sigma}_{11}/J_1)^{2m}+(1-\hat{\sigma}_{22}/J_1)^{2m}+(1-\hat{\sigma}_{33}/J_1)^{2m}}} & (\text{if } i=j) \\ 0 & (\text{if } i\neq 0) \end{cases} \tag{42}$$

Failure surfaces using Eq. (35) in conjunction with Eq. (42) coincides with the extended Mises surface for $m=0$ and generates surfaces very close to the Lade–Duncan and the Matsuoka–Nakai strength surfaces for $m=0.51$ and $m=0.66$ respectively [Fig. 7(a)]. A failure surface close to the critical state surface predicted by the t_{ij}-clay model can be generated for $m=0.555$ [Fig. 7(b)]. For m value higher than 0.66, the strength surface moves inside the Mohr–Coulomb surface at triaxial extension [Fig. 6(b)]. It implies that the angle of internal friction under triaxial extension is lower than that of triaxial compression condition, which is not supported by the experimental evidence. Also, convexity of the strength surface in the ordinary stress space is not guaranteed. But modeling is still possible for $m > 0.66$, since it forms a circular shape in the modified stress space. Fig. 8 also shows that various strength criteria can be closely generated by the proposed concept by varying m.

In the t_{ij}-concept the tensor a_{ij} is related to the direction cosines of the SMP. Thus, its expression cannot be changed. On the other hand, b_{ij} is not related to any physical plane like the SMP and is an arbitrary function of the ordinary stress and its invariants. But its properties are similar to a_{ij}. Both a_{ij} and b_{ij} are the isotropic tensors at isotropic stress conditions. If the stress condition is anisotropic and if the principal stresses are in the order $\hat{\sigma}_{11} \geqslant \hat{\sigma}_{22} \geqslant \hat{\sigma}_{33}$, then the principal values of both a_{ij} and b_{ij} should be in the reverse order ($\hat{a}_{11} \leqslant \hat{a}_{22} \leqslant \hat{a}_{33}$ and $\hat{b}_{11} \leqslant \hat{b}_{22} \leqslant \hat{b}_{33}$). If the principal values of b_{ij} are in the same order ($\hat{b}_{11} \geqslant \hat{b}_{22} \geqslant \hat{b}_{33}$) as the ordinary stress $\hat{\sigma}_{11} \geqslant \hat{\sigma}_{22} \geqslant \hat{\sigma}_{33}$, then the predicted strengths will be higher than those predicted by the extended Mises criterion under triaxial extension and true triaxial conditions.

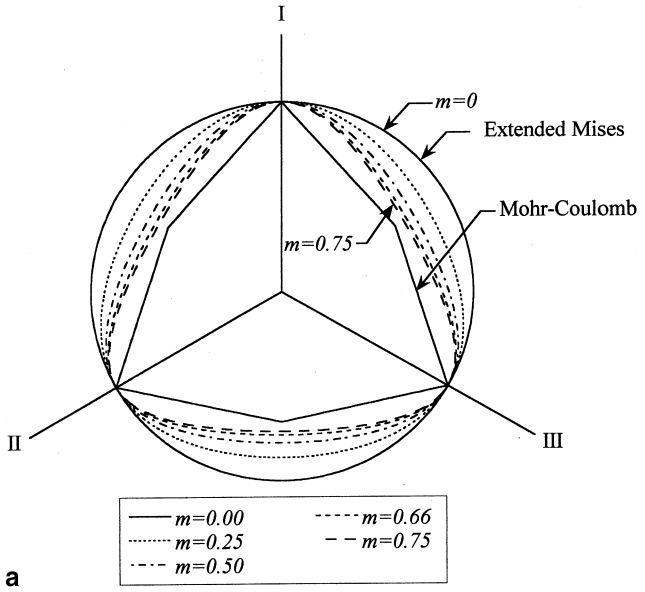

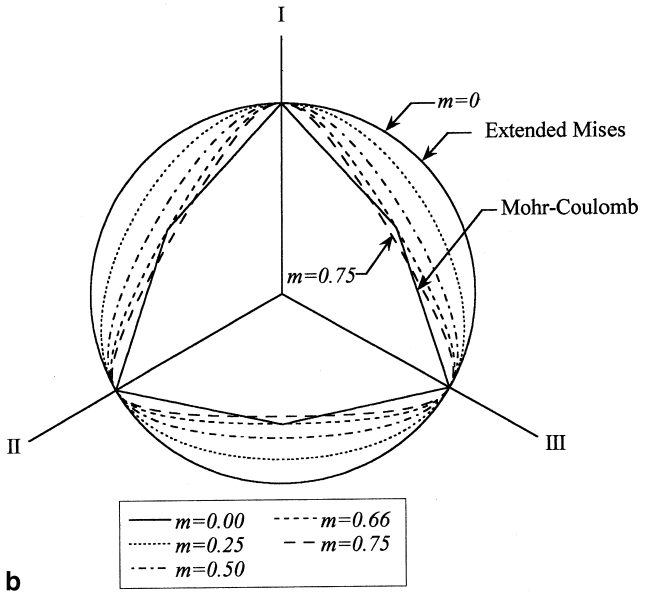

Fig. 6. (a) Failure surfaces using Eq. (39). (b) Failure surfaces using Eq. (40).

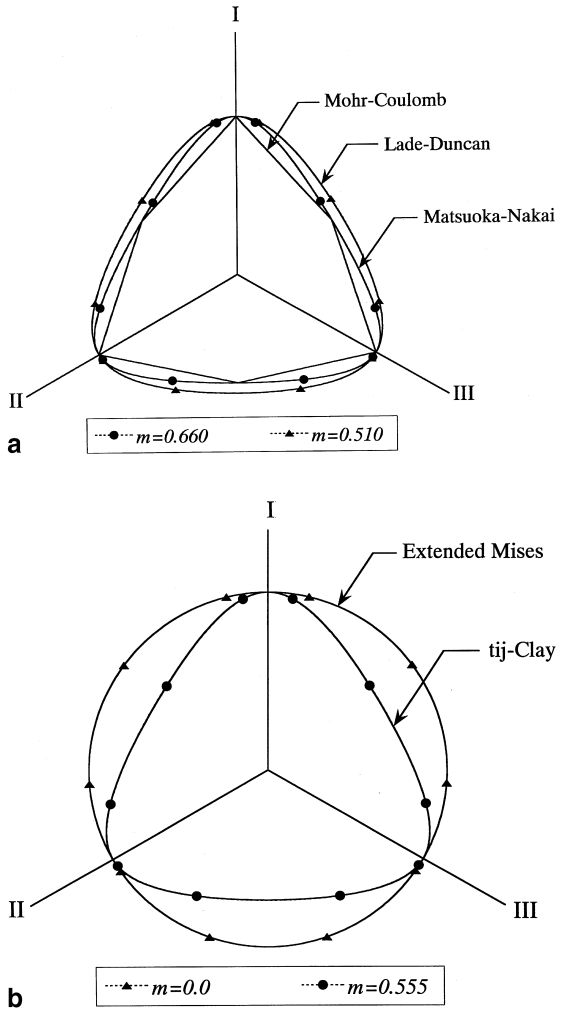

Fig. 7. (a) Generation of strength surfaces close to the Matsuoka–Nakai and the Lade–Duncan surfaces using Eq. (42). (b) Generation of strength surfaces close to the extended Mises and the critical state surface of the t_{ij}-clay model using Eq. (42).

2.3. Work conjugate stress and strain increment components

Now, we will show that the proposed stress and strain increment quantities are properly work conjugate and in the process, we will recapitulate the Cam clay and t_{ij}-clay work equations. When a cubical soil element supporting effective stresses σ_{ij} is subjected to arbitrary plastic strain increments $d\varepsilon_{ij}^{p}$, then the external plastic work done per unit volume is

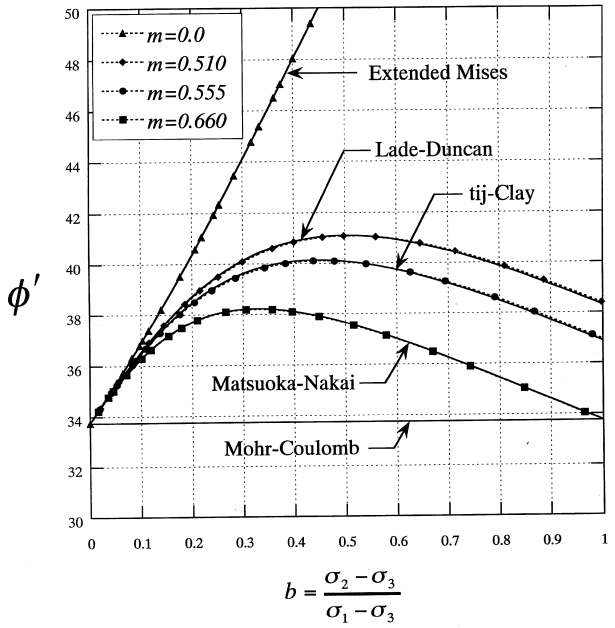

Fig. 8. Generation of various strength criteria using Eq. (42).

$$\mathrm{d}W_{\mathrm{ext}} = \sigma_{ij}\,\mathrm{d}\varepsilon_{ij}^{\mathrm{p}}. \tag{43}$$

If the stresses are principal stresses and if we assume the principal directions of the plastic strain increments coincide with the principal directions of the stresses, then the above work equation becomes

$$\mathrm{d}W_{\mathrm{ext}} = \sigma_1\,\mathrm{d}\varepsilon_1^{\mathrm{p}} + \sigma_2\,\mathrm{d}\varepsilon_2^{\mathrm{p}} + \sigma_3\,\mathrm{d}\varepsilon_3^{\mathrm{p}}. \tag{44}$$

The Cam clay plastic work equation can be given by

$$\mathrm{d}W_{\mathrm{ext}} = \sigma_1\,\mathrm{d}\varepsilon_1^{\mathrm{p}} + \sigma_2\,\mathrm{d}\varepsilon_2^{\mathrm{p}} + \sigma_3\,\mathrm{d}\varepsilon_3^{\mathrm{p}} = p\,\mathrm{d}\varepsilon_{\mathrm{v}}^{\mathrm{p}} + q\,\mathrm{d}\varepsilon_{\mathrm{d}}^{\mathrm{p}} \tag{45}$$

The above equation is not valid for any arbitrary plastic strain increments but valid only if the following equation holds.

$$\frac{\sigma_2 - \sigma_3}{\sigma_1 - \sigma_3} = \frac{\mathrm{d}\varepsilon_2^{\mathrm{p}} - \mathrm{d}\varepsilon_3^{\mathrm{p}}}{\mathrm{d}\varepsilon_1^{\mathrm{p}} - \mathrm{d}\varepsilon_3^{\mathrm{p}}}. \tag{46}$$

In other words, the Cam-clay work equation holds if the direction of the strain increment vector coincides with the direction of stress vector on the π-plane. This can be better understood from Fig. 9(a) that shows the π-plane section of the plastic potential in the ordinary stress space, which is a circle. Also, it can be seen that the direction of the current stress vector (radial direction) and the normal to the plastic potential are identical. If the flow rule is given such that the plastic strain increment

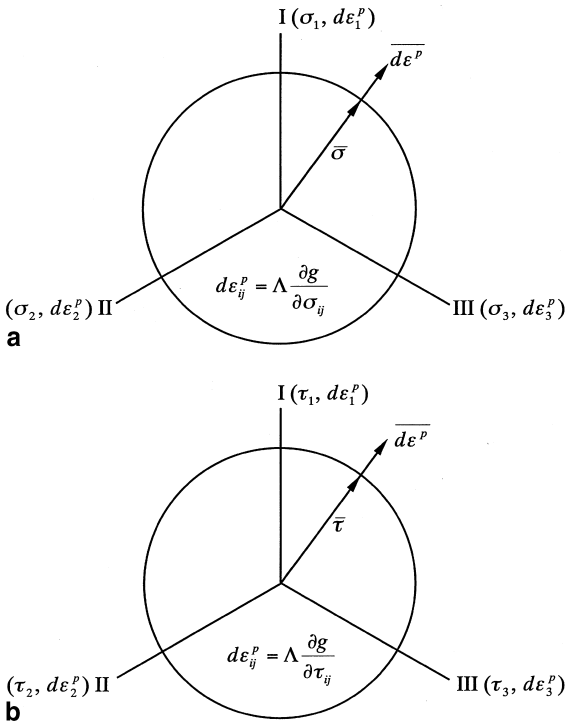

Fig. 9. (a) Cam-clay plastic potential, stress and strain increment vectors on the deviator plane in the ordinary stress space. (b) Plastic potential, modified stress and strain increment vectors on the deviator plane in the modified stress space.

vector is directed to the outward normal to the plastic potential in the same stress space, it will automatically satisfy Eqs. (45) and (46). Hence, the Cam-clay stress components (p and q) and plastic strain increments (d_v^p and d_d^p) are work conjugate.

Since, the principal directions of the proposed stress (τ_{ij}) are coaxial with the principal directions of the ordinary stress (σ_{ij}) and the principal directions of the plastic strain increment (d_{ij}^p), the plastic work equation using proposed stress and strain increment quantities becomes

$$dW_{ext}^{**} = \tau_1 \, d\varepsilon_1^p + \tau_2 \, d\varepsilon_2^p + \tau_3 \, d\varepsilon_3^p = \tau_m \, d\varepsilon_v^p + \tau_s \, d\varepsilon_s^p. \tag{47}$$

Likewise the Cam-clay model, Eq. (47) is valid if

$$\frac{\tau_2 - \tau_3}{\tau_1 - \tau_3} = \frac{d\varepsilon_2^p - d\varepsilon_3^p}{d\varepsilon_1^p - d\varepsilon_3^p} \tag{48}$$

Fig. 9(b) shows the π-plane section of the plastic potential in the modified stress space, which is a circle. So, the normal to the plastic potential and the direction of current modified stress vector on the π-plane will be the same. Using the analogy of the Cam-clay model, the stress and the strain increment quantities will become work [not the ordinary work but the one given by [Eq. (47)] conjugate if the plastic strain increment vector is outward normal to the plastic potential in the modified stress space. Since, the plastic potential for an elastoplastic model we shall formulate in the next section will be given using modified stress and the flow rule will also be given in the modified stress space, the stress and strain increment quantities will become work conjugate. An analytical verification of Eq. (47) can be made in the same way as the Cam-clay model.

On the other hand, in the t_{ij}-concept, principal directions of t_{ij} are coaxial with the principal directions of the ordinary stress (σ_{ij}) and the principal directions of the plastic strain increment ($d\epsilon_{ij}^{p}$) and the corresponding work equation is given by [6]:

$$dW_{ext}^{*} = t_1\, d\varepsilon_1^{p} + t_2\, d\varepsilon_2^{p} + t_3\, d\varepsilon_3^{p} = t_N d\varepsilon_{SMP}^{*p} + t_S\, d\gamma_{SMP}^{*p}. \tag{49}$$

From the middle part of the above equation, it can be seen that the modified stress and the ordinary strain increments give the plastic work according to the t_{ij}-concept. In the right-hand side of the above equation, the stress quantities t_N and t_S are respectively the components of modified stress (t_{ij}) along a_{ij} and perpendicular to it. The conjugate strain increments $d\varepsilon_{SMP}^{*p}$ and $d\gamma_{SMP}^{*p}$ respectively are obtained by resolving the ordinary plastic strain increments along a_{ij} and perpendicular to it. Flow rule of the t_{ij}-clay model also links the ordinary plastic strain increments to the modified stress (Table 1).

It is to note that objectivity of the stress and the strain increment parameters has also been verified numerically. The plastic work given by the Eqs. (47) and (49) are not the ordinary work as Eq. (44) but the plastic work according to the respective concepts. Thus, we can conclude that the proposed stress and strain increment quantities are properly work conjugate for the proposed expressions of $\hat{b}_{ij}$ and probably for many other expressions.

3. Model formulation

Since the proposition of the Cam clay, numerous models have been proposed to simulate various aspects of soil behavior. Namely, dependency of the direction of plastic flow on the direction of loading, inherent anisotropy induced during the formation of the ground and the stress-induced anisotropy due to shear and stabilization of strains during cyclic loading. However, we shall formulate a simple model for clay within the conventional framework of the critical state soil mechanics and call it as the MS-Clay model. Here, MS stands for the modified stress.

First we assume the following decomposition of the total strain increments:

$$d\varepsilon_{ij} = d\varepsilon^{e}_{ij} + d\varepsilon^{p}_{ij}. \tag{50}$$

The elastic strain increment follows the generalized Hooke's law.

$$d\varepsilon^{e}_{ij} = \frac{1+v_e}{E_e} d\sigma_{ij} - \frac{v_e}{E_e} d\sigma_{kk}\delta_{ij}. \tag{51}$$

The plastic strain increment is given by the flow rule in the modified stress space (since, the proposed modified stresses and the plastic strain increments are conjugate in the modified stress space) as given below.

$$d\varepsilon^{p}_{ij} = \frac{\partial g}{\partial \tau_{ij}}. \tag{52}$$

The proportionality constant Λ can be evaluated from the consistency condition given using either ordinary or the modified stress as follows:

$$= \frac{\frac{\lambda-\kappa}{1+e_0}\frac{\partial f}{\partial \tau_{ij}} d\tau_{ij}}{\frac{\partial g}{\partial \tau_{kk}}} = \frac{\frac{\lambda-\kappa}{1+e_0}\frac{\partial f}{\partial \sigma_{ij}} d\sigma_{ij}}{\frac{\partial g}{\partial \tau_{kk}}}. \tag{53}$$

Soil parameters λ and κ in the above equations are the slopes of the normal consolidation and unloading–reloading lines of a e vs.ln τ_m (or e vs.ln p) plot and e_o is the reference void ratio.

Without giving an expression for the internal energy dissipation and without equating it with the external work done [Eq. (47)], we intuitively write the stress–dilatancy relation using the proposed stress and strain increment quantities as

$$D = \frac{d\varepsilon^{p}_{v}}{d\varepsilon^{p}_{s}} = \frac{\chi_f^{\beta} - \chi^{\beta}}{\alpha \chi^{\beta-1}}, \tag{54}$$

where χ_f is the stress ratio at the critical state. The above stress–dilatancy relation introduces two new parameters (α and β) to retain completeness and generality. It has similarity with the stress–dilatancy relations of the original ($\alpha=\beta=1$) and the modified ($\alpha=\beta=2$) Cam-clay models and the t_{ij}-clay model ($\beta=1$) though the stress and strain increment variables are different. The original Cam clay gives relatively flexible, and the modified Cam clay gives stiffer initial response in general and there is no control over it. However, using the proposed stress–dilatancy relation and adjusting the parameters α and β, desired initial response can be obtained. These parameters also control the continuity and smoothness of the plastic potential. A continuous and smooth plastic potential ensures gradual drop in stiffness when shearing starts from isotropic stress condition.

Some parametric analyses of Eq. (54) are shown in Fig. 10. Fig. 10(a) shows stress–dilatancy curves keeping $\alpha=$constant and varying β and Fig. 10(b) shows those keeping $\beta=$constant and varying α. It can be seen from these figures that

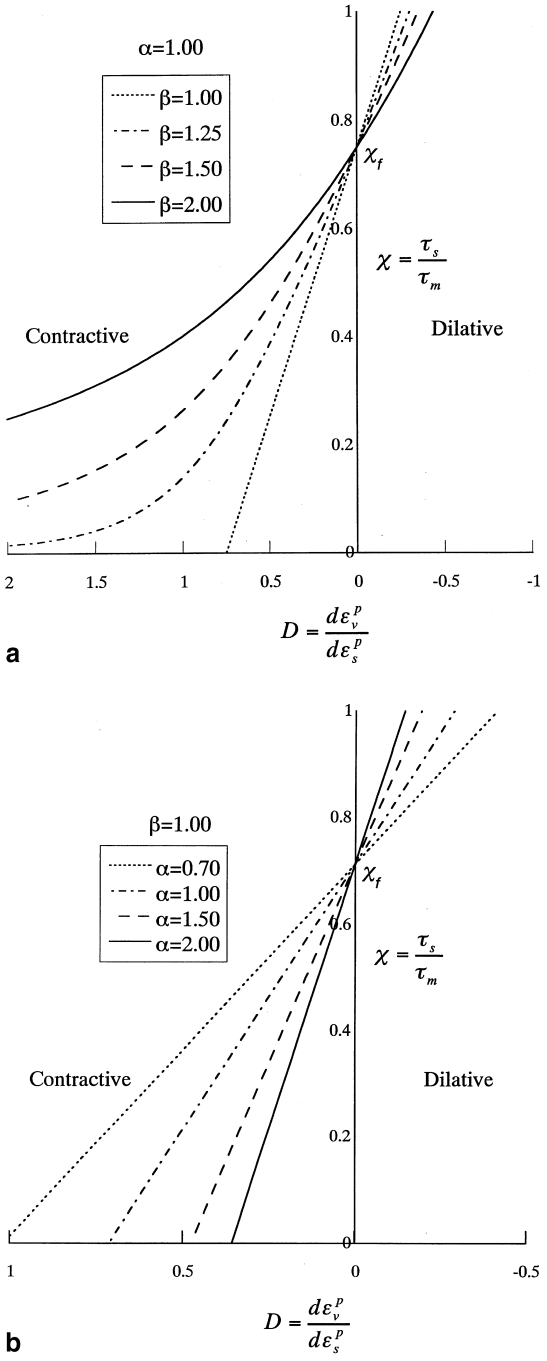

Fig. 10. (a) Variation of stress–dilatancy with parameter β. (b) Variation of stress–dilatancy with parameter α.

when α increases, stress–dilatancy curve moves toward the dilative zone and as a consequence stress-strain response becomes flexible if the yield function remains the same or if the associated flow is assumed. On the contrary, when β increases, stress–dilatancy become more contractive and stress-strain response becomes stiffer.

In the constitutive modeling of geomaterials non-associated flow rule is frequently used to suppress excessive volumetric strains in the analyses of over-consolidated or cyclically loaded soils. Since, the model is primarily intended to simulate normally consolidated clay behavior, it is reasonable to assume associated flow rule. Also, associated flow rule is simple and satisfies Drucker's stability postulate. Considering the normality condition (associated flow rule) and integrating Eq. (54) yield and plastic potential functions can be obtained as Eqs. (55) and (56).

$$g \equiv f = \frac{\lambda - \kappa}{1 + e_0}\left[\ln\frac{\tau m}{\tau_{m0}} + \frac{1}{\beta}\left(\frac{\chi}{\chi_f}\right)^{\beta}\right] - \varepsilon_{\mathrm{v}}^{\mathrm{p}} = 0 \quad \text{for } \alpha = 1, \tag{55}$$

$$g \equiv f = \frac{\lambda - \kappa}{1 + e_0}\left[\ln\frac{\tau_m}{\tau_{m0}} + \frac{\alpha}{\beta(\alpha - 1)}\ln\left\{1 + (\alpha - 1)\left(\frac{\chi}{\chi_f}\right)^{\beta}\right\}\right] - \varepsilon_{\mathrm{v}}^{\mathrm{p}} = 0 \quad \text{for } \alpha \neq 1. \tag{56}$$

Functions similar to the Eqs. (55) and (56) have been used in the original t_{ij}-clay model [8] with $\beta = 1$ and in an extended t_{ij}-clay model [13,14], a function similar to Eq. (55) has been used, which implicitly assumes $\alpha = 1$.

Shapes of the plastic potentials corresponding to the stress–dilatancy relations of Fig. 10 are shown in Fig. 11. For the linear stress–dilatancy relations ($\beta = 1$), the tip of the plastic potential is singular irrespective of α [Fig. 11(b)] like the original Cam clay and the t_{ij}-clay models. Also, if $\alpha < 1$ then the second logarithm term of Eq. (56) becomes indeterminate if $\chi \geqslant \chi_f/(1-\alpha)^{1/\beta}$, which is a very high stress ratio. In the analyses of normally or lightly over-consolidated soils, peak stress ratios are much below than the above limiting value. But for the heavily over-consolidated soils, peak stress ratios (χ) can be higher than $\chi_{\mathrm{f}}/(1-\alpha)^{1/\beta}$. If $\alpha \geqslant 1$ then such indeterminate situation disappears but singularity at the tip of the plastic potential remains.

Singularity at the tip of the plastic potential disappears if $\beta > 1$. Fig. 11(a) shows plastic potentials for $\alpha = 1.0$ and varying values of β. As seen in this figure, tip of the plastic potential becomes more rounded as β increases and consequently stress-strain response becomes stiffer. From the foregoing discussion, we can conclude that for a smooth plastic potential using Eq. (54) the following inequality must be satisfied.

$$\alpha \geqslant 1, \quad \beta > 1. \tag{57}$$

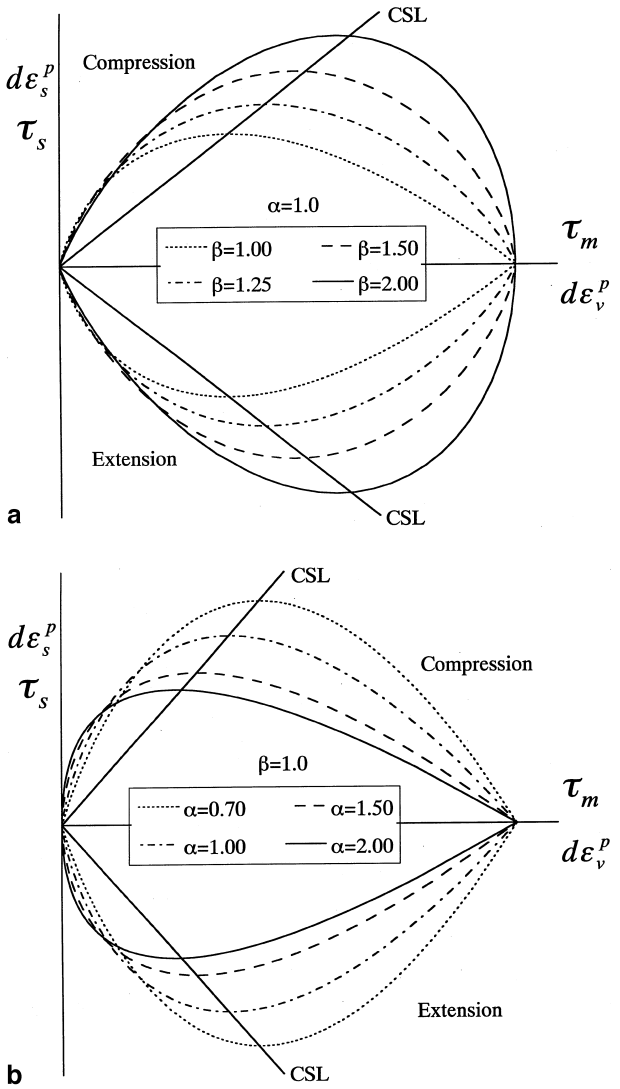

Fig. 11. (a) Variation of the shapes of plastic potentials with β. (b) Variation of the shapes of plastic potentials with α.

4. Experimental observations and numerical simulations

4.1. Testing method

Saturated, remolded and normally consolidated Fujinomori clay was used in the triaxial and true triaxial experiments. Physical properties of the Fujinomori clay are

liquid limit $w_L = 41\%$, plastic limit $w_p = 23\%$ and the specific gravity $G_s = 2.67$. At first, the clay powder was mixed with de-aired water and one-dimensionally consolidated under a pressure of 49 kpa. Water content after one-dimensional consolidation was about 34%. Cylindrical samples of diameter 5.0 cm and 10.0 cm high were used in the triaxial tests. After placing the samples in the triaxial apparatus these were isotropically consolidated under effective confining pressures of 196 kpa with back pressures of 98 kpa. No significant anisotropy due to initial one-dimensional consolidation was observed after isotropic consolidation. Then, the samples were sheared at constant mean stress under drained condition at an axial strain rate of about 1% per day.

Nakai et al. [15] performed drained true triaxial tests with fixed and hinged connections between the vertical loading plate and the loading ram. The data presented here are those of the hinged connection. In these tests cubical (10.5 cm $\times$ 10.3 cm $\times$ 7.0 cm) samples were used, which were isotropically consolidated under effective mean stresses of 196 kpa. For the detailed testing procedure refer to the paper mentioned above. Like the triaxial tests, true triaxial samples were also sheared at constant mean stress. Axial strain rate in these tests was about 0.8% per day.

Stress paths of the triaxial and true triaxial tests are shown in Fig. 12. Here, θ indicates the angle between σ_a-axis and the corresponding radial stress path on the deviator plane. The angle $\theta = 0^\circ$ and $\theta = 180^\circ$ denote the stress paths of triaxial compression and extension respectively. Other stress paths ($\theta = 15^\circ$, $\theta = 30^\circ$ and $\theta = 45^\circ$) denote three different principal stresses.

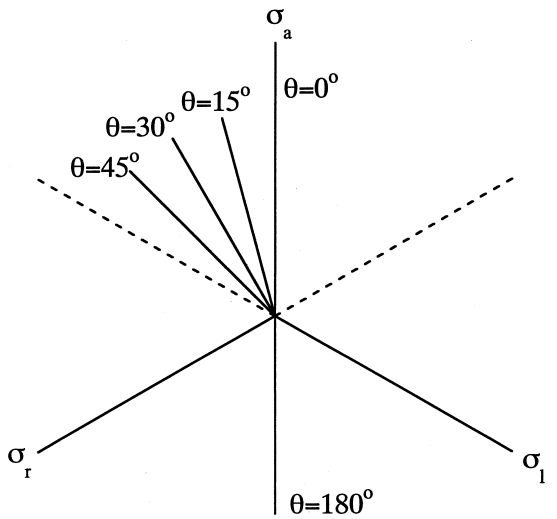

Fig. 12. Stress paths of the triaxial and the true triaxial tests on the octahedral plane.

Since, the proposed model cannot consider the effect of loading direction on the direction of plastic flow, triaxial test results of increasing or decreasing mean stress and the rotation of principal axes (torsional shear test) are not presented here.

4.2. Soil parameters

A total of seven parameters are required for the proposed model while, the Cam clay needs only four and the t_{ij}-Clay model requires five parameters. However, the increased number of parameters may not be a drawback of the proposed model because no further experiments are necessary to determine the parameters α, β and m. Also, these parameters give flexibility to fit the observed stress-strain response and the strength of soils. Experimental determination of the parameter m would be very costly and time consuming because it needs many true triaxial test data. So, it should be assumed to fit the desired failure surface in the modeling.

Since, the t_{ij}-clay model predicts closely the observed shear behavior of clay [15], performance of the proposed model has been checked against the t_{ij}-clay model by using the critical state surface of the t_{ij}-clay model as the failure surface for the proposed model ($m = 0.555$).

Values of the soil parameters of the Fujinomori clay for various models are listed in Table 2.The first two soil parameters C_t and C_e can be determined from the slopes of the normal-consolidation and unloading–reloading lines of an isotropic consolidation test using reference void ratio e_0. The strength parameter φ'_{comp} can be determined from a triaxial compression test. Poisson's ratio v_e is assumed to be zero. The parameter α of the t_{ij}-Clay model has been determined not from the slope of the observed stress–dilatancy but so chosen that it produces the same confining pressure as the original Cam-clay model at the critical state in the analysis of an undrained triaxial compression test. Parameters α and β of the proposed model have been determined by a semi trial–error method. Various values of α have been assumed and β values are calculated using Eqs. (55) and (56) for a given plastic volumetric strain. Amount of plastic volumetric strain can be estimated from the triaxial test

Table 2
Soil parameters of Fujinomori clay for various models

Parameter	Cam-Clay	t_{ij}-Clay	MS-clay
$C_t = \lambda/(1+e_0)$	4.44×10^{-2}	4.44×10^{-2}	4.44×10^{-2}
$C_e = k/(1+e_0)$	0.47×10^{-2}	0.47×10^{-2}	0.47×10^{-2}
ϕ'_{comp}	33.7°	33.7°	33.7°
v_e	0.0	0.0	0.0
α	–	0.7	1.0
β	–	–	1.24
m	–	–	0.555

that has been performed to determine the strength parameter. To be more precise, elastic volumetric strain for the triaxial test can be estimated using Hooke's law and can be deducted from the total volumetric strain to calculate the plastic volumetric strain. Using these combinations of α and β, analyses for the triaxial compression test have been made, then the combination that best fits the observed response is chosen as the parameters.

4.3. Performance of the model

First of all, we verified that there is no effect of stress level in the proposed model by analyzing triaxial compression tests at different confining pressures, which is the same as the Cam clay and the t_{ij}-clay models.

Figs. 13–18 show the observed and the predicted responses in the triaxial and true triaxial tests. In these figures principal strains are plotted against the stress ratio (q/p), and the volumetric strain (ε_v) is plotted against the major principal strain. Also, solid curves in these figures are the predicted responses by the proposed model and broken curves are those by the t_{ij}-clay model. Simulations by the original Cam-clay model were shown by Nakai et al. [15], which do not fit the observed responses in general and are excluded from the figures for neatness. Figs. 13 and 14 correspond to the triaxial compression and extension tests respectively and Figs. 15–18 are those of the true triaxial tests.

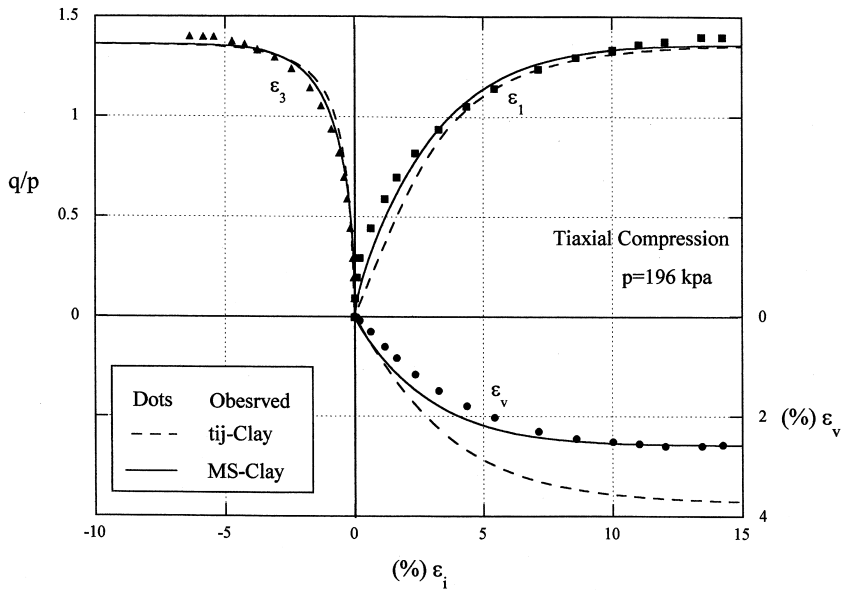

Fig. 13. Observed in the triaxial compression test and the predicted responses by the t_{ij}-clay and the proposed models.

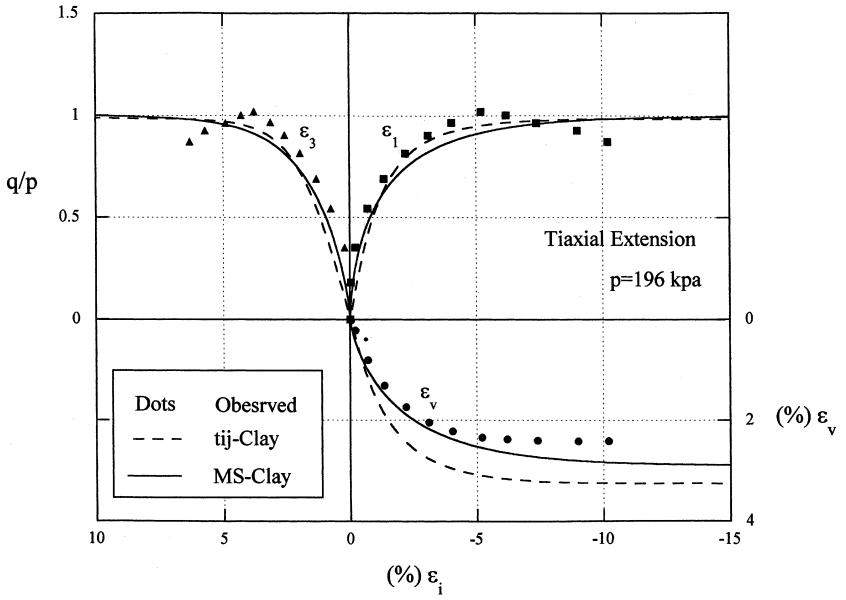

Fig. 14. Observed in the triaxial extension test and the predicted responses by the t_{ij}-clay and the proposed models.

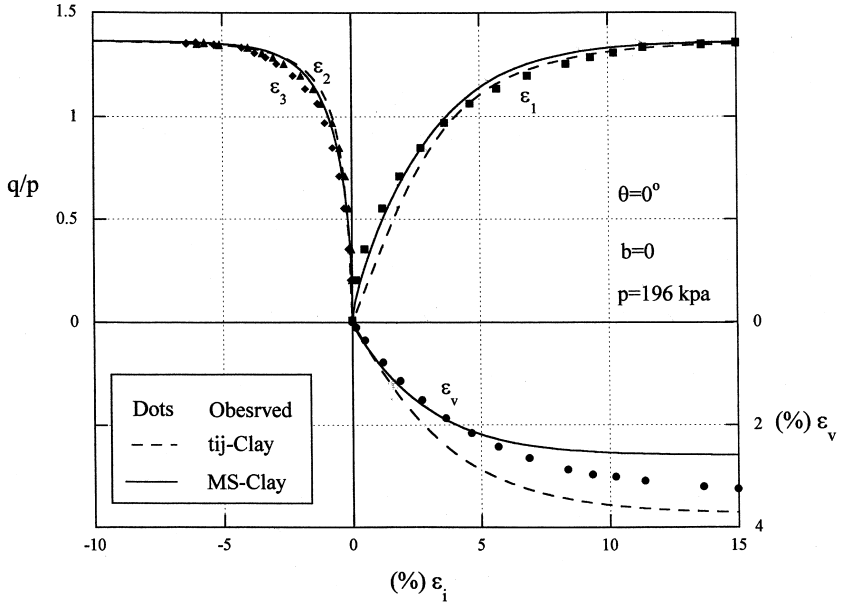

Fig. 15. Observed in the true triaxial test ($\theta = 0°$) and the predicted responses by the t_{ij}-clay and the proposed models.

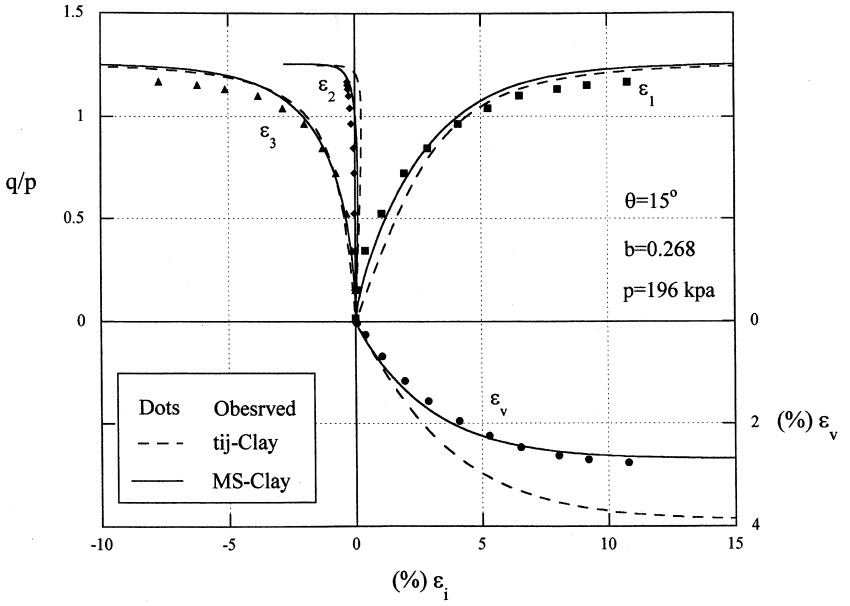

Fig. 16. Observed in the true triaxial test ($\theta = 15°$) and the predicted responses by the t_{ij}-clay and the proposed models.

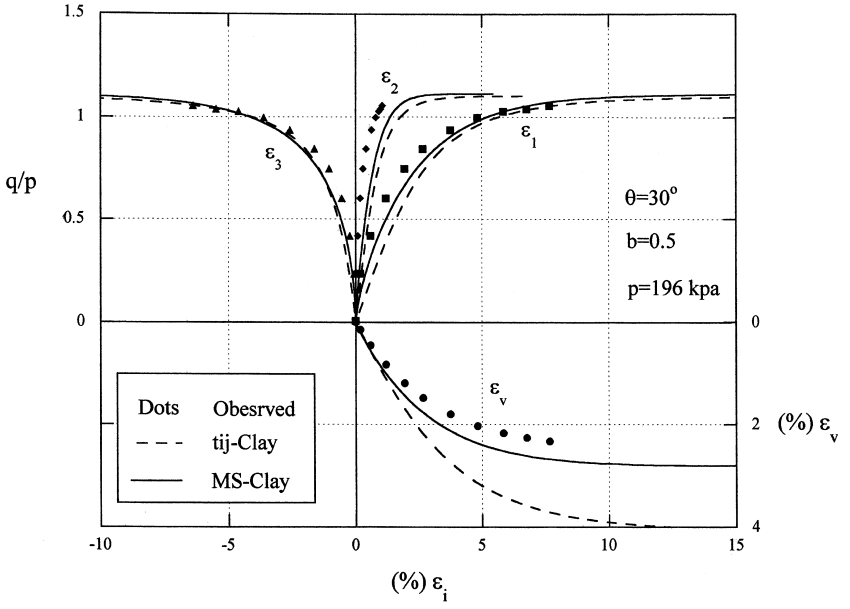

Fig. 17. Observed in the true triaxial test ($\theta = 30°$) and the predicted responses by the t_{ij}-clay and the proposed models.

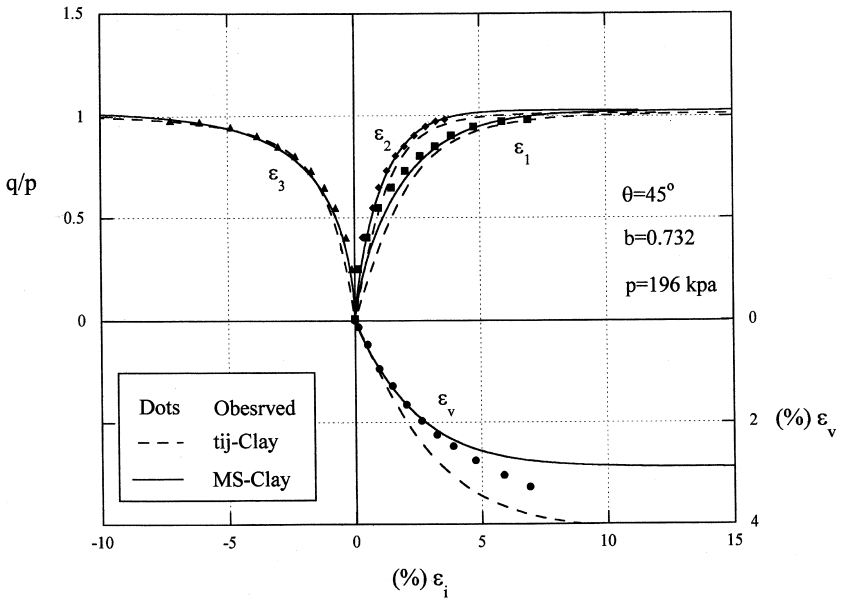

Fig. 18. Observed in the true triaxial test ($\theta = 45°$) and the predicted responses by the t_{ij}-clay and the proposed models.

From all these figures, it is clear that the proposed model closely predicts the observed stress-strain behavior. Also, responses at low stress ratio are smooth due to the use of the proposed plastic potential, whose tip is rounded for $\beta > 1$ and consequently stiffness changes gradually. On the other hand, the t_{ij}-clay model slightly over predicts volumetric strain and the initial responses are flexible. The strengths predicted by both the models are almost the same and slightly higher than those observed under true triaxial and triaxial extension conditions because we used the critical state surface of the t_{ij}-clay model as the failure surface of the proposed model.

The observed stress–dilatancy relations using the proposed stress and strain increment quantities are shown in Fig. 19, which are aligned in a narrow band with scatters at low stress ratios. This scatter may be due to the presence of elastic strains in the observed responses, whose proportions are comparable to the plastic strains at low stress ratios. Solid line in this figure is the stress–dilatancy relation used in the proposed model, which closely resemble the observed trend.

Fig. 20(a) shows the directions of the observed strain increment vectors in the true triaxial tests under three different principal stresses ($\theta = 15°$, 30° and 45°) on the deviator plane. The length of each vector is given by the ratio of the shear strain increment ($\delta\varepsilon_d$) to the stress ratio increment $[\delta(q/p)]$. It is clear from this figure that the directions of the observed strain increment vectors deviate from the direction of shear stress (radial direction) with a definite trend as the stress ratio increases. Fig. 20(b) shows the directions of the predicted strain increment vectors by the proposed

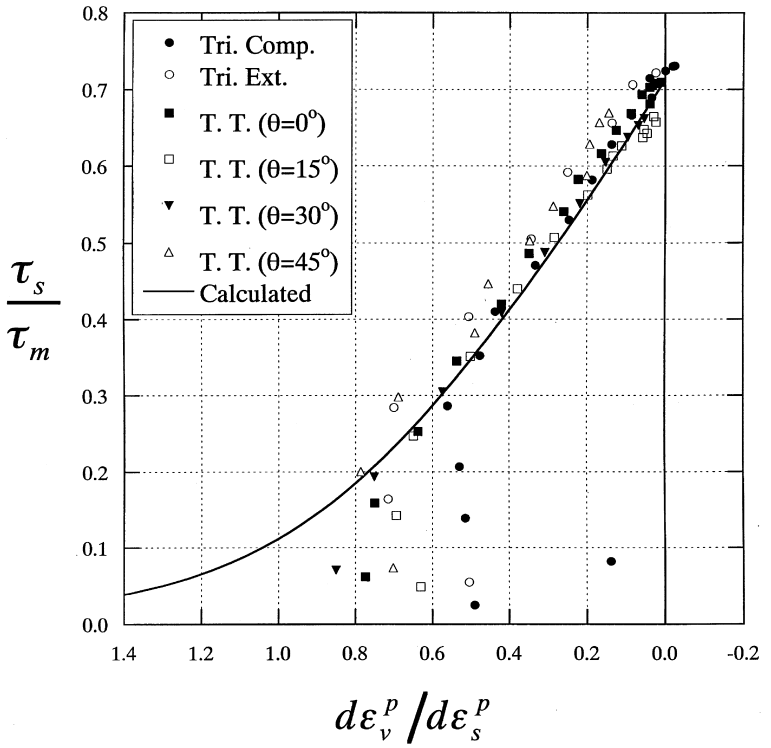

Fig. 19. Observed stress–dilatancy in various tests and calculated one for the proposed model.

model, which are in good agreement with the observed trend. Nakai et al. [15] have also showed the predicted responses by the t_{ij}-clay and the Cam-clay models. It has been observed that the t_{ij}-clay also expresses the observed trend. On the other hand, calculated strain increment vectors by the Cam clay are always directed in the radial direction, which is far apart from the observed trend.

Fig. 21 shows the observed stress conditions at peak stress ratio on the deviator plane. In this figure solid squares correspond to the test data of the true triaxial apparatus (rectangular parallelepiped specimen) and the solid circles are those of the triaxial apparatus (cylindrical specimen). The observed stress condition at failure using the true triaxial apparatus at $\theta = 0°$ slightly deviates from $\sigma_2 = \sigma_3$ line, since the two horizontal stresses could not equalized perfectly. Even though the different sets of the triaxial test data from those of Nakai are presented in this paper, but in these tests too, observed strengths are slightly higher than those observed using true triaxial apparatus, which are consistent with the triaxial test data presented by Nakai. Shibata and Karube [16] and Lade and Musante [17] reported a similar trend. In this figure Mohr–Coulomb, Matsuoka–Nakai strength criteria and the

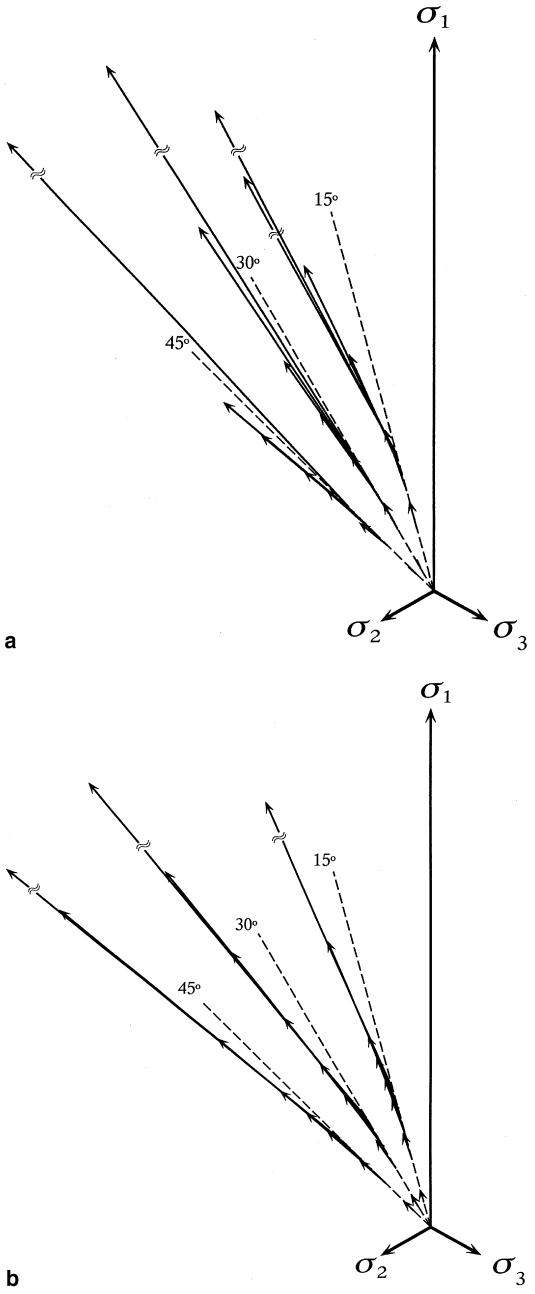

Fig. 20. (a) Directions of the observed strain increments on the octahedral plane. (b) Directions of the calculated strain increments on the octahedral plane.

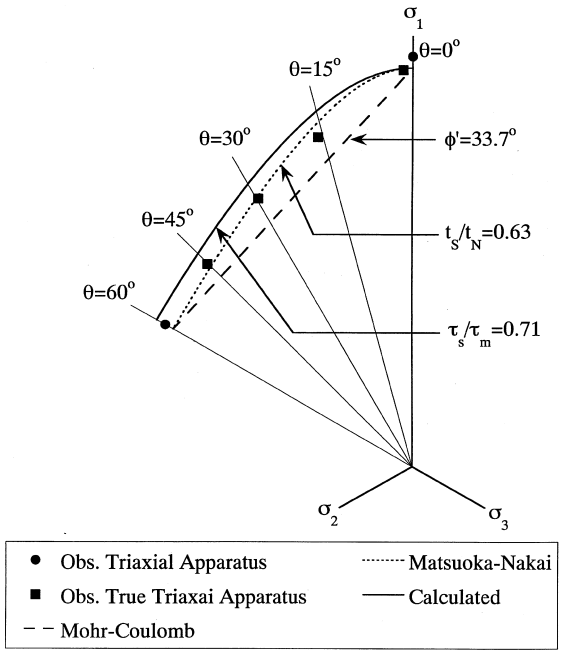

Fig. 21. Observed and predicted strengths in the triaxial and the true triaxial tests.

strength criteria used in the proposed model are plotted. The strength criterion used in the proposed model slightly over predicts strengths under true triaxial and triaxial extension conditions, which can also be seen in the stress-strain curves.

5. Conclusions

This paper introduces a modeling approach using modified stress to consider the influence of intermediate principal stress, which can adopt wide variety of strength criteria and is consistent with the critical state concept. It has similarity with the t_{ij}-concept, which also uses modified stress but the underlying principles are quite different. In the t_{ij}-concept stress parameters are the components of the modified stress (t_{ij}) normal and parallel to the SMP and the conjugate strain increment components are the components of the ordinary strain increments along the directions corresponding to the stress parameters. On the other hand, in the proposed concept, mean and deviator components of the modified stress are considered as the stress parameters and the conjugate strain increments are the volumetric and the deviator strains respectively. Use of these parameters ensures the critical state to be reached

when stress ratio (χ) reaches a constant value ($\chi = \chi_f$) independent of the relative magnitude of the intermediate principal stress.

An expression for the tensor b_{ij}, which transforms the ordinary stresses, controls the shape of the failure surface and influences the stress–dilatancy relation has been suggested, but other expressions may also give good results.

A compact stress–dilatancy relation is also introduced, which gives a continuous and smooth plastic potential. Two new parameters pertaining to the proposed stress–dilatancy relation control the shape and influence the model response and can be adjusted to fit the observed response.

In order to check the validity of the proposed model triaxial and true triaxial tests have been analyzed. Predictions by the proposed model show good agreements with the observed responses. As a demonstration of the proposed concept, the critical state surface of the t_{ij}-clay model is considered as the failure surface, but other strength surfaces can also be implemented in a similar way. Though the proposed model is for the normally consolidated clay it can also be extended to simulate the over-consolidated and the cyclically loaded clay behavior.

Appendix

The main hurdle in using the proposed model would be the determination of the partial derivatives under general 3-D stress conditions, which can be determined directly or by transformation as follows:

$$\frac{\partial g}{\partial \tau_{ij}} = \frac{\partial g}{\partial \hat{\tau}_{kl}} \frac{\partial \hat{\tau}_{kl}}{\partial \tau_{ij}} = Q_{ik} Q_{jl} \frac{\partial g}{\partial \hat{\tau}_{kl}}, \tag{A1}$$

$$\frac{\partial f}{\partial \sigma_{ij}} = \frac{\partial f}{\partial \hat{\sigma}_{kl}} \frac{\partial \hat{\sigma}_{kl}}{\partial \sigma_{ij}} = Q_{ik} Q_{jl} \frac{\partial f}{\partial \hat{\sigma}_{kl}}, \tag{A2}$$

Where $\partial g/\partial \hat{\tau}_{kl}$ and $\partial f/\partial \hat{\sigma}_{kl}$ are the derivatives in a different coordinate system, preferably in the principal stress space. Partial derivatives can also be calculated directly using chain rule as in Eq. (A.3)Eq. (A.5).

$$\frac{\partial g}{\partial \tau_{ij}} = \frac{\partial g}{\partial \tau_m} \frac{\partial \tau_m}{\partial \tau_{ij}} + \frac{\partial g}{\partial \chi} \frac{\partial \chi}{\partial \chi_{kl}} \frac{\partial \chi_{kl}}{\partial \tau_{ij}}. \tag{A3}$$

Eq. (55) or (56) gives the plastic potential, its derivatives are:

$$\frac{\partial g}{\partial \tau_m} = \frac{1}{\tau_m}, \frac{\partial \tau_m}{\partial \tau_{ij}} = \frac{\delta_{ij}}{3} \quad \delta_{ij} = 1 \text{ if } i = j, \quad \delta_{ij} = 0 \text{ if } i \neq j,$$

$$\frac{\partial g}{\partial \chi}=\frac{\alpha}{\chi}\frac{\left(\frac{\chi}{\chi_f}\right)^{\beta}}{1+(\alpha-1)\left(\frac{\chi}{\chi_f}\right)^{\beta}},\ \frac{\partial \chi}{\partial \chi_{kl}}=\frac{\partial\sqrt{\chi_{kl}\chi_{kl}}}{\partial \chi_{kl}}=\frac{2\chi_{kl}}{2\sqrt{\chi_{kl}\chi_{kl}}}=\frac{\chi_{kl}}{\chi},\ \frac{\partial \chi_{kl}}{\partial \tau_{ij}}$$
$$=\frac{\partial}{\partial \tau_{ij}}\left(\frac{\tau_{kl}-\tau_m\delta_{kl}}{\tau_m}\right)=\frac{\partial}{\partial \tau_{ij}}\left(\frac{\tau_{kl}}{\tau_m}-\delta_{kl}=\frac{\delta_{ik}\delta_{jl}}{\tau_m}-\frac{\tau_{kl}}{\tau_m^2}\frac{\delta_{ij}}{3}\right.$$
$$=\frac{1}{\tau_m}\left\{\delta_{ik}\delta_{jl}-(\chi_{kl}+\delta_{kl})\frac{\delta_{ij}}{3}\right\}.$$

Substituting above findings in Eq. (A.3) gives Eq. (A.4), which is the required partial derivative of the plastic potential.

$$\frac{\partial g}{\partial \tau_{ij}}=\frac{1}{\tau_m}\frac{\delta_{ij}}{3}+\frac{\alpha}{\chi}\frac{\left(\frac{\chi}{\chi_f}\right)^{\beta}}{1+(\alpha-1)\left(\frac{\chi}{\chi_f}\right)^{\beta}}\cdot\frac{\chi_{kl}}{\chi}\cdot\frac{1}{\tau_m}\left\{\delta_{ik}\delta_{jl}-(\chi_{kl}+\delta_{kl})\frac{\delta_{ij}}{3}\right\}. \tag{A4}$$

Now, $\frac{\partial f}{\partial \sigma_{ij}}$ can be derived as follows:

$$\frac{\partial f}{\partial \sigma_{ij}}=\frac{\partial f}{\partial \tau_{kl}}\frac{\partial \tau_{kl}}{\partial \sigma_{ij}}. \tag{A5}$$

$\partial f\partial\tau_{kl}$ of the above equation can be derived similarly as $\partial g/\partial\tau_{ij}$ and is given below.

$$\frac{\partial f}{\partial \tau_{kl}}=\frac{1}{\tau_m}\frac{\delta_{kl}}{3}+\frac{\alpha}{\chi}\frac{\left(\frac{\chi}{\chi_f}\right)^{\beta}}{1+(\alpha-1)\left(\frac{\chi}{\chi_f}\right)^{\beta}}\cdot\frac{\chi_{pq}}{\chi}\cdot\frac{1}{\tau_m}\left\{\delta_{kp}\delta_{lq}-(\chi_{pq}+\delta_{pq})\frac{\delta_{kl}}{3}\right\}, \tag{A6}$$

$$\frac{\partial \tau_{kl}}{\partial \sigma_{ij}}=\frac{\partial(b_{km}\sigma_{ml})}{\partial \sigma_{ij}}=b_{km}\delta_{im}\delta_{jl}+\sigma_{ml}\frac{\partial b_{km}}{\partial \sigma_{ij}}, \tag{A7}$$

$$\frac{\partial b_{ij}}{\partial \sigma_{kl}}=\frac{\partial b_{ij}}{\partial \hat{b}_{mn}}\frac{\partial \hat{b}_{mn}}{\partial \hat{\sigma}_{pq}}\frac{\partial \sigma_{pq}}{\partial \sigma_{kl}}=Q_{im}Q_{jn}Q_{kp}Q_{lq}\frac{\partial \hat{b}_{mn}}{\partial \hat{\sigma}_{pq}}. \tag{A8}$$

The principal values of b_{ij} are given by Eq. (42), then the fourth order tensor $\partial\hat{b}_{ij}/\partial\hat{\sigma}_{kl}$can be obtained as follows:

$$\frac{\partial \hat{b}_{ij}}{\partial \hat{\sigma}_{kl}}=\hat{b}_{ij}\left(\frac{1}{k}\frac{\partial K}{\partial \hat{\sigma}_{kl}}-\frac{m}{J_1}\right)\quad \text{if } i=j=k=l,$$

$$\frac{\partial \hat{b}_{ij}}{\partial \hat{\sigma}_{kl}} = \hat{b}_{ij}\left[\frac{1}{k}\frac{\partial K}{\partial \hat{\sigma}_{kl}} - \frac{m\hat{\sigma}_{ij}}{J_1^2(1-\hat{\sigma}_{ij}/J_1)}\right] \quad \text{if } i=j,\ \ k=l,\ \ i\neq k.$$

It is important to note that in the principal space $\hat{b}_{ij}=0$ if $i\neq j$ but the rate of changes $\partial\hat{b}_{ij}/\partial\hat{\sigma}_{kl}\neq 0$ if $i=k$ and $j=l$ or $i=l$ and $j=k$, which are given below.

$$\frac{\partial \hat{b}_{ij}}{\partial \hat{\sigma}_{kl}} = \left|\frac{\hat{b}_{ik}-\hat{b}_{jl}}{2}\right| \quad \text{if } i=k,\ \ j=l,\ \ i\neq j,$$

$$\frac{\partial \hat{b}_{ij}}{\partial \hat{\sigma}_{kl}} = \left|\frac{\hat{b}_{il}-\hat{b}_{jk}}{2}\right| \quad \text{if } i=l,\ \ j=k,\ \ i\neq j,$$

$$\frac{\partial \hat{b}_{ij}}{\partial \hat{\sigma}_{kl}} = 0 \quad \text{else.}$$

Here,

$$K = \frac{1}{\sqrt{(1-\hat{\sigma}_{11}/J_1)^{2m}+(1-\hat{\sigma}_{22}/J_1)^{2m}+(1-\hat{\sigma}_{33}/J_1)^{2m}}}$$

and if $i=j$ then

$$\frac{\partial K}{\partial \hat{\sigma}_{ij}} = \frac{Km}{J_1} - \frac{K^3 m}{J_1}\left[(1-\delta_{li})(1-\hat{\sigma}_{11}/J_1)^{2m-1}+(1-\delta_{2i})(1-\hat{\sigma}_{22}/J_1)^{2m-1}+(1-\delta_{3i})(1-\hat{\sigma}_{33}/J_1)^{2m-1}\right]$$

else

$$\partial K/\partial\hat{\sigma}_{ij}=0.$$

Substituting the above derivatives in Eq. (A.8) and using Eqs. (A.5)–(A.8), $\partial f/\partial\sigma_{ij}$ can be determined.

References

[1] Roscoe KH, Schofield AN, Thurairajah A. Yielding of clays in states wetter than critical. Geotechnique 1963;13(3):211–40

[2] Roscoe KH, Burland JB. On the generalized stress-strain behavior of "wet" clay. In: Heyman J, Leckie FA, editors. Engineering plasticity. Cambridge, UK: Cambridge University Press, 1968:535–609

[3] Lade PV, Duncan JM. Elastoplastic stress–strain theory for cohesionless soil. Proceedings ASCE 101(GT10) 1975:1037–53

[4] Matsuoka H, Nakai T. Stress-deformation and strength characteristics of soil under three different principal stresses. Proc. JSCE 1974;232:59–70
[5] Nakai T, Matsuoka H. Shear behaviors of sand and clay under three dimensional stress condition. Soils and Foundations 1983;23(2):26–42
[6] Nakai T, Mihara Y. A new mechanical quantity for soils and its application to elastoplastic constitutive models. Soils and Foundations 1984;24(2):82–94
[7] Narasimhan MNL. Principles of continuum mechanics. Wiley, New York, 1993
[8] Nakai T, Matsuoka H. A generalized elastoplastic constitutive model for clay in three-dimensional stresses. Soils and Foundations 1986;26(3):81–98
[9] Nakai T. An isotropic hardening elastoplastic model for sand considering the stress path dependency in three-dimensional stresses. Soils and Foundations 29(1):119–37
[10] Nakai T, Hoshikawa T. Kinematic hardening model for clay in three dimensional stresses. Computer Methods and Advances in Geomechanics 1991;1:655–60
[11] Nakai T, Funada T. Constitutive model for sand considering induced and inherent anisotropy. In: International symposium on numerical models in geomechanics, NUMOG IV, 1992:63–72
[12] Wood DM. Soil behaviour and critical state soil mechanics. Cambridge, UK: Cambridge University Press, 1990
[13] Chowdhury EQ, Nakai T. A generalized model for clay under monotonic and cyclic loading conditions. In: Pietruszczak S, Pande GN, editors. Numerical models in geomechanics, NUMOG VI, Balkema, Montreal, Canada, 1997:111–16
[14] Nakai T, Chowdhury EQ, Tawada M, Nishida K. Deformation and strength of clay under triaxial and torsional shear. In: Asaoka A, Adachi T, Oka F, editors. Deformation and progressive failure in geomechanics, IS-Nagoya. Japan: Elsevier, 1997:127–32
[15] Nakai T, Matsuoka H, Okuno N, Tsuzuki K. True triaxial tests on normally consolidated clay and analysis of the observed shear behavior using elastoplastic constitutive models. Soils and Foundations 1986;26(4):67–78
[16] Shibata T, Karube D. Influence of the variation of the intermediate principal stress on the mechanical properties of normally consolidated clays. In: Proceedings of the Sixth ICSMFE, vol. 1, 1965:359–63
[17] Lade PV, Musante HM. Three-dimensional behavior of remolded clay. Proc. ASCE 104(GT 2) 1978:193–209